ISPRS Annals of the Photogrammetry, Remote Sensing and Spatial Information Sciences, Volume X-G-2025
ISPRS Geospatial Week 2025 “Photogrammetry & Remote Sensing for a Better Tomorrow…”, 6–11 April 2025, Dubai, UAE

Accuracy assessment of DSM in mountainous forest areas generated from GF-7 stereo images assisted by ATLAS/ICESat-2

Junfeng Xie[1], Xiaomeng Yang[1], Qingxing Yue[1], Jiyi Chen[1], Jun Peng[1]

[1]Land Satellite Remote Sensing Application Center, Ministry of Natural Resources of P.R. China

Keywords: DSM generation, GF-7 stereo images, Accuracy evaluation, ATLAS/ICESat-2, mountainous forest area

Abstract

The successful launch of the GaoFen-7 (GF-7) satellite has made it possible to achieve sub-meter-level three-dimensional mapping. However, most current studies focus on accuracy evaluating of GF-7 stereo mapping in bare land, and less on its performance in mountainous forest areas. This study aims to explore the potential of ground control points (GCPs) from the Ice, Cloud, and Land Elevation Satellite-2 (ICESat-2) to enhance the accuracy of GF-7 digital surface models (DSM) in forested areas, and further evaluate the performance of GF-7 stereo mapping in mountainous forest areas. First, the GCPs was extracted from ATL03 based on the direction adaptive OPTICS ground surface detection method. Then, with the assistance of Google Earth (GE), fine screening was applied to extract bare GCPs in forested areas, which were called ATLGE GCPs. Finally, the ATLGE GCPs were used as elevation control points, combined with GF-7 stereo images to generate the forest area DSM, which was called GF-7 DSM_ATLGE. To compare and analyze the potential of ATLGE GCPs in improving the accuracy of GF-7 forest DSM, SRTM and SLA03 were employed as elevation controls data to generate GF-7 DSM_SRTM and GF-7 DSM_SLA03, respectively. The elevation accuracy of the three DSMs was quantitatively evaluated using the DSM obtained from field-surveyed plots. The results showed that while GF-7 DSM_SRTM, GF-7 DSM_SLA03, and GF-7 DSM_ATLGE all effectively represented forest features, their accuracy varied significantly. Specifically, the elevation RMSE of GF-7 DSM_SRTM was 11.87 m, GF-7 DSM_SLA03 reached 4.78 m, and GF-7 DSM_ATLGE reached 2.99 m, showing a significant improvement. These results not only demonstrate the effectiveness of ATLGE GCPs in enhancing the elevation accuracy of GF-7 DSMs in forest areas, but also highlight the stereo mapping capability of GF-7 stereo images under controlled conditions in complex mountainous forest areas.

1. Introduction

The Gao Fen-7 (GF-7) satellite, China's first civilian optical stereo mapping satellite with sub-meter resolution, is designed to provide high spatial resolution and temporal resolution, as well as high-precision Earth observation capabilities. It facilitates the rapid acquisition of large-scale, high-precision digital surface model (DSM) for 1:10,000 scale topographic mapping (Zhu et al., 2024). When GF-7 stereo images are applied to forestry research, they can generate large-area, continuous forest DSMs, providing a solid data foundation for quantifying vegetation structure. However, due to the complexity of forest terrain and features, research on GF-7 DSMs in forested areas has been limited. Additionally, without ground control points (GCPs), GF-7 stereo imagery-derived DSMs in forests are insufficient for supporting high-precision quantitative applications. Therefore, reliable GCPs are essential to enhancing the usability of GF-7 DSMs in forest areas and exploring the potential of GF-7 stereo mapping for forestry.

The acquisition methods for GCPs needed to generate DSMs from stereo images are mainly divided into two categories (Du et al., 2023). The first method involves using differential handheld Global Navigation Satellite System (GNSS), Global Navigation Satellite System-Real-Time Kinematic (GNSS-RTK), and other surveying instruments to collect GCPs in the field. While this method provides high-precision GCPs, it is costly, especially in complex terrains such as dense forest areas, where field collection of GCPs presents significant challenges. The second method, which has become widely used in recent years, involves using auxiliary data to replace field-collected GCPs. For example, Zhou et al. utilized Shuttle Radar Topography Mission (SRTM) data as auxiliary elevation information to jointly process ZY-3 stereo images through regional bundle adjustment, improving block adjustment accuracy and meeting China’s vertical accuracy requirements for 1:25,000 scale mapping (Zhou et al., 2018). Liu et al. used GF-7 laser data as elevation control and performed bundle adjustment with stereo images, improving the elevation accuracy of bare-earth DSMs by approximately 1 m (Liu et al., 2022). The rapid development of satellite lidar technology has provided more options for obtaining reliable GCPs. Zhu et al. introduced Advanced Topographic Laser Altimeter System (ATLAS) as GCPs, reducing the Root Mean Square Error (RMSE) of bare-earth GF-7 DSMs to 1.35 m, highlighting ATLAS's great potential in enhancing DSMs elevation accuracy (Zhu et al., 2023). Additionally, with the advancement of Google Earth (GE) technology and the accumulation of high-resolution multi-temporal imagery, Ni et al. developed a method to collect GCPs using GE multi-temporal imagery, lowering the RMSE of GF-7 DSMs to 1.5 m, providing a reliable data foundation for accurately assessing forest terrain and canopy height in future studies (Ni et al., 2024).

Most current research primarily focuses on exploring the representation of bare land using GF-7 stereo images under controlled conditions. It is still challenging to explore the use of ATLAS bare GCPs to improve the accuracy of GF-7 DSM mountain forest. This study aims to utilize GE images as an auxiliary data, combined with the ground surface detection method based on direction adaptive OPTICS (Xie et al, 2024), to finely screen a small number of ATLAS bare GCPs (ATLGE GCPs) in forested areas. ATLGE GCPs are used as elevation constraints to generate the GF-7 DSM in combination with GF-7 stereo images, and is called GF-7 DSM_ATLGE. The research explores the potential of ATLGE GCPs to improve the elevation accuracy of GF-7 forest DSMs and further assess the observational capabilities of the GF-7 satellite in complex mountainous forest areas.

This contribution has been peer-reviewed. The double-blind peer-review was conducted on the basis of the full paper.
https://doi.org/10.5194/isprs-annals-X-G-2025-981-2025

2. Datasets

2.1 Gaofen-7(Gf-7) Stereo Images and Laser Footprints

GF-7 is China's first sub-meter-resolution stereo mapping satellite, equipped with high-resolution dual-linear-array stereo optical cameras and a satellite-borne laser altimetry system. It is capable of capturing high-spatial-resolution optical stereo observation data and high-precision laser altimetry data, aiming at 1:10,000-scale mapping. The dual-linear-array stereo optical cameras were composed of a forward Charge-Coupled Device (CCD) camera with an angle of ±26° and a backward CCD camera at -5°. It could effectively acquire 20 km wide panchromatic stereoscopic images (0.8 m resolution for the forward view and 0.65 m for the backward view), as well as multi-spectral images with a 2.6m resolution (Zhu et al, 2023). The GF-7 laser altimetry system was equipped with four lasers, two footprint cameras, and one optical axis monitoring camera. This system was primarily designed to assist the stereo optical cameras in enhancing the accuracy of uncontrolled mapping. It utilized a dual-beam laser operating in a 3/6 Hz measurement mode to observe the ground simultaneously, while the footprint cameras captured images of both the laser footprints and the terrain. The optical axis monitoring camera was used to capture the laser footprints and track any changes in the optical axis.
This study used three pairs of GF-7 stereo images processed to Level 1A, with their spatial coverage illustrated in Figure 1. Track 17285 was acquired in December 2022, track 4606 in September 2020, and track 13644 in April 2022. Additionally, for the purposes of comparative analysis, the Level 3 laser data (SLA03) corresponding to these three pairs of stereo images was utilized, as shown in Figure 1.

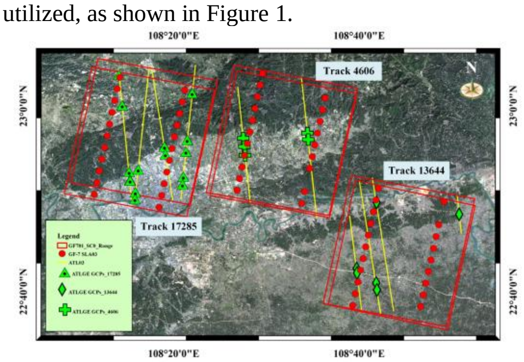

Figure 1. Experimental data distribution

2.2 ICESat-2/ATLAS Data

NASA successfully launched the Ice, Cloud, and Land Elevation Satellite-2 (ICESat-2) in September 2018. It was equipped with ATLAS, which emitted laser pulses at a repetition rate of 10 kHz. This system captured overlapping laser footprints with a diameter of 17.5m spaced at 0.7m intervals. The high precision and dense sampling make it have great potential in GCPs acquisition. ICESat-2 products were categorized into Level 1, Level 2, Level 3A, and Level 3B, based on differences in processing levels and application scenarios. For this study, ATL03 was chosen as the research object because the signal located in the forest bare earth needed to be obtained as the GCPs, which required high density. The distribution of ATL03 was illustrated by the yellow markings in Figure 1.

2.3 Reference Data

In the experimental area around Nanning, Guangxi, a detailed survey was conducted on 34 plots (20 m × 30 m). For each plot, the four corner points were measured using the GNSS to serve as GCPs, with a positioning accuracy better than 0.5 m. The Trimble TX8 and the Riegl 1560i system were used to scan the plots, and the two datasets were registered to obtain the complete point clouds. Utilizing the LAStools software, the point clouds were processed through denoising and classification to generate a DSM with a 1m resolution, which was then utilized for experimental validation in this study.

3. Method

This study aims to explore the potential of ICESat-2 GCPs to improve the accuracy of GF-7 DSM in forested areas, and further evaluate the performance of GF-7 stereo mapping in complex mountainous forest areas. To this end, a high-precision DSM generation method for mountainous forest areas was proposed, utilizing ICESat-2 to assist GF-7 stereo images. The workflow was illustrated in Figure 2.

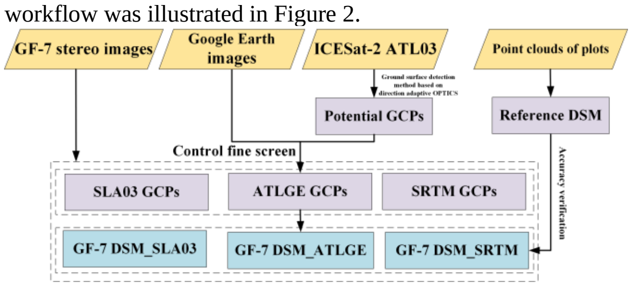

Figure 2. The workflow of this study

As shown in Figure 2, the ICESat-2 GCPs for bare land in the forest area obtained by combining GE with the ground surface detection method based on direction adaptive OPTICS. These GCPs were referred to as ATLGE GCPs. Using ATLGE GCPs, SLA03, and SRTM as elevation controls, the GF-7 stereo images were combined to generate three DSMs, named GF-7 DSM_ATLGE, GF-7 DSM_SLA03, and GF-7 DSM_SRTM, respectively. The elevation accuracy of the DSMs was validated using field-surveyed plots, which also provided an indirect assessment of the accuracy of ATLAS GCPs. Consequently, this study was divided into three parts: generation of ATLGE GCPs, generation of GF-7 DSMs, and comparison and validation of DSMs elevation accuracy.

3.1 Generation of ATLGE GCPs

For the multi-track ATL03 data within the study area, high-quality data that were evenly distributed across the image coverage were selected whenever possible. Because the instability of forests can easily reduce the ability of canopy elevation control points to improve DSM, this study decided to use bare GCPs in forest areas as elevation control for DSM. The ground surface detection method based on direction adaptive OPTICS (Xie et al, 2024) was employed to obtain the ground surface from ATL03, treating these as potential GCPs. To ensure that the GCPs located in the bare land of the forest area, the potential GCPs located in easily identifiable and stable positions, such as artificial structures and small natural objects, were selected as ATLGE GCPs with reference to GE.

3.2 Generation of GF-7 DSMs

The GF-7 stereo images provide Rational Polynomial Coefficient (RPC) parameter files, which are used to derive the generic geometric model Rational Function Model (RFM). The RFM establishes the mapping relationship between image coordinates and object coordinates using rational polynomials, as shown in Equation (1) (Fraser and Hanley., 2005). However, the initial RPCs lack physical significance and have low accuracy (Grodecki et al., 2003). To improve the accuracy of the generic geometric model for stereo images, the block adjustment method is commonly used to compensate for the radiometric transformation parameters

.

$$\begin{cases} r = \frac{p_1(X,Y,Z)}{p_2(X,Y,Z)} \\ c = \frac{p_3(X,Y,Z)}{p_4(X,Y,Z)} \end{cases} \quad (1)$$

$$\begin{cases} \Delta c = a_0 + a_1 c + a_2 r \\ \Delta r = b_0 + b_1 c + b_2 r \end{cases} \quad (2)$$

Where p_1、p_2、p_3、p_4 are the RPCs; (r,c) are the image coordinates; (X,Y,Z) is the object coordinates; $(\Delta c\ ,\Delta r)$ are the compensation of the image coordinates;a_i,b_i(i = 0, 1, 2) are the affine transformation coefficients (Zhu et al, 2023).

Currently, the commonly used block adjustment method can be categorized into two types: with GCPs and without GCPs. In the case of the latter, tie points are selected from the GF-7 stereo images, and space intersection is used to calculate the three-dimensional ground coordinates in the target space, forming virtual GCPs. Although this method is low-cost, its elevation accuracy does not meet the requirements for practical applications. In recent years, more studies have focused on the block adjustment method with GCPs. This method is further divided based on the type of GCPs used (Zhu et al., 2023).

Block adjustment using open-source geographic data. This method aligns commonly used open-source data, such as GE and SRTM DEM, with GF-7 stereo images to extract homologous points that contain both horizontal and elevation coordinates, treating them as GCPs.

Block adjustment using laser data homologous to the stereo images. Taking GF-7 stereo images as an example, the laser footprint images serve as a bridge to locate the corresponding positions of laser altimeter points (LAPs) pixel coordinates within the stereo images. LAPs are then used as elevation control points to achieve a combined block adjustment with the stereo images (Zhou et al., 2018).

Block adjustment using high-precision heterologous GCPs. The core of this method lies in using high-precision GCPs to constrain the elevation at the corresponding locations of the stereo images. GCPs can be collected through field surveys, but achieving a balance between accuracy and cost can be challenging. Alternatively, they can be obtained from open-source satellite laser altimetry, such as ICESat-2, which offers high accuracy at a lower cost.

As described in Section 1, this study took ICESat-2 as the research object to obtain ATLGE GCPs by controlling the fine screen. Using the Space Data Processor (SDP), independently developed by the Land Satellite Remote Sensing Application Center of the Ministry of Natural Resources of the People's Republic of China, ATLGE GCPs were used as elevation constraints and the 2m accuracy base map as planar constraints for the GF-7 stereo images, producing the GF-7 DSM_ATLGE. To analyze the ability of ATLGE GCPs to improve the accuracy of forest DSMs, this study used SRTM DEM and GF-7 SLA03 as elevation controls, while 2m accuracy base map served as a planar control, constraining the generation of GF-7 DSM_SRTM and GF-7 DSM_SLA03.

3.3 Comparison and Validation of DSMs Elevation Accuracy

Using field-surveyed plots as a reference, the elevation accuracy of GF-7 DSM_ATLGE, GF-7 DSM_SRTM, and GF-7 DSM_SLA03 was evaluated by introducing two metrics: bias and root mean square error (RMSE), as shown in Equations (3), (4).

$$Bias = \frac{\sum_{i=1}^{n}(H_{i,j} - H_{i,ref})}{n} \quad (3)$$

$$RMSE = \sqrt{\frac{\sum_{i=1}^{n}(H_{i,j} - H_{i,ref})^2}{n}} \quad (4)$$

where n represents the number of plots within the current DSM range, $j = 1,2,3$ represent DSMs generated under three different control conditions: GF-7 DSM_ATLGE, GF-7 DSM_SRTM, and GF-7 DSM_SLA03. Here, $H_{i,ref}$ denotes the mean elevation of the $i - th$ plot, while $H_{i,j}$ represents the mean elevation at the corresponding location in the $j - th$ DSM.

4. Result and Discussion

4.1 Generation of ATLGE GCPs

Figure 3 illustrated the potential GCPs acquired by the directional adaptive OPTICS. From Figures 3 (a) and (b), it is evident that, based on visual interpretation, the potential GCPs detected by this method were highly reliable. To further screen high-precision and distinct bare land GCPs in forested areas, GE was introduced. By identifying intersections between the potential GCPs and features such as artificial structures and small natural objects, the three-dimensional coordinates of the potential GCPs were considered as the intersection coordinates, forming the ATLGE GCPs, as shown by the yellow markers in Figure 4 (a) to (c).

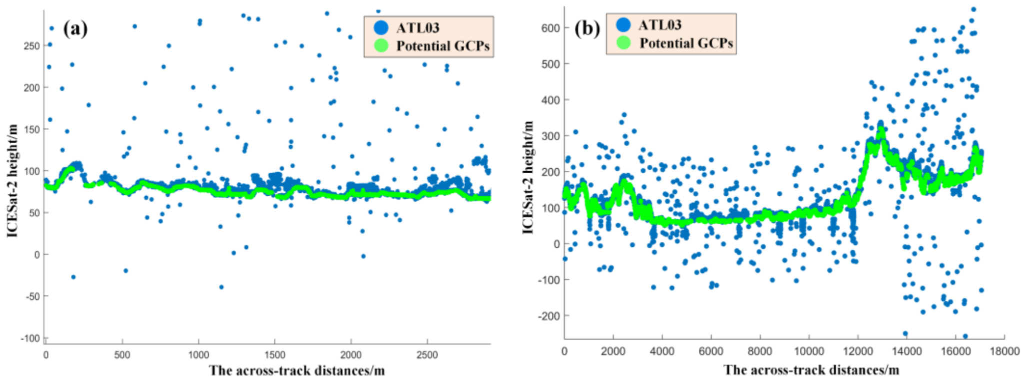

Figure 3. Results of extracting potential GCPs from ATL03 data.

Figure 4. Intersection points (yellow markers) between features in GE and potential GCPs from ATL03.

4.2 Comparison and Validation of DSMs Elevation Accuracy

The DSMs generated directly by the SDP exhibited null values in waters and areas with weak textures. In this study, after patching the null values of DSMs with the help of Advanced Spaceborne Thermal Emission and Reflection Radiometer Global Digital Elevation Model Version 3 (ASTER GDEM V3) data, GF-7 DSM_ATLGE, GF-7 DSM_SRTM, and GF-7 DSM_SLA03 generated by block adjustment under three different elevation control conditions were obtained as shown in Figure 5. Visual interpretation revealed minimal differences in detail richness and elevation continuity among the three DSMs generated from the same stereo images, with only certain variations in the range of elevation values.

Using DSM generated from point clouds processing of field-surveyed plots within the study area as a reference, the elevation accuracy of the three DSMs was validated, as detailed in Table 1. From Table 1, it is evident that the RMSE of GF-7 DSM_SRTM was relatively high, reaching 11.87m. As the accuracy of the elevation control data increased, the elevation accuracy of the DSMs improved correspondingly. Specifically, the RMSE of GF-7 DSM_SLA03 reached 4.78m, while the RMSE of GF-7 DSM_ATLGE reached 2.99 m. It is clear that GF-7 DSM_ATLGE exhibited superior elevation accuracy compared to the other two DSMs, indirectly demonstrating the feasibility of using ATLGE GCPs as elevation control points. Additionally, it is worth noting that for stereo images from 4606 and 13644, even though the number of ATLGE GCPs was significantly less than that of SLA03 GCPs (as shown in Figure 1), the RMSE of GF-7 DSM_ATLGE within the field-surveyed plots still outperformed that of GF-7 DSM_SLA03, further highlighting the superiority of ATLGE GCPs as elevation control points.

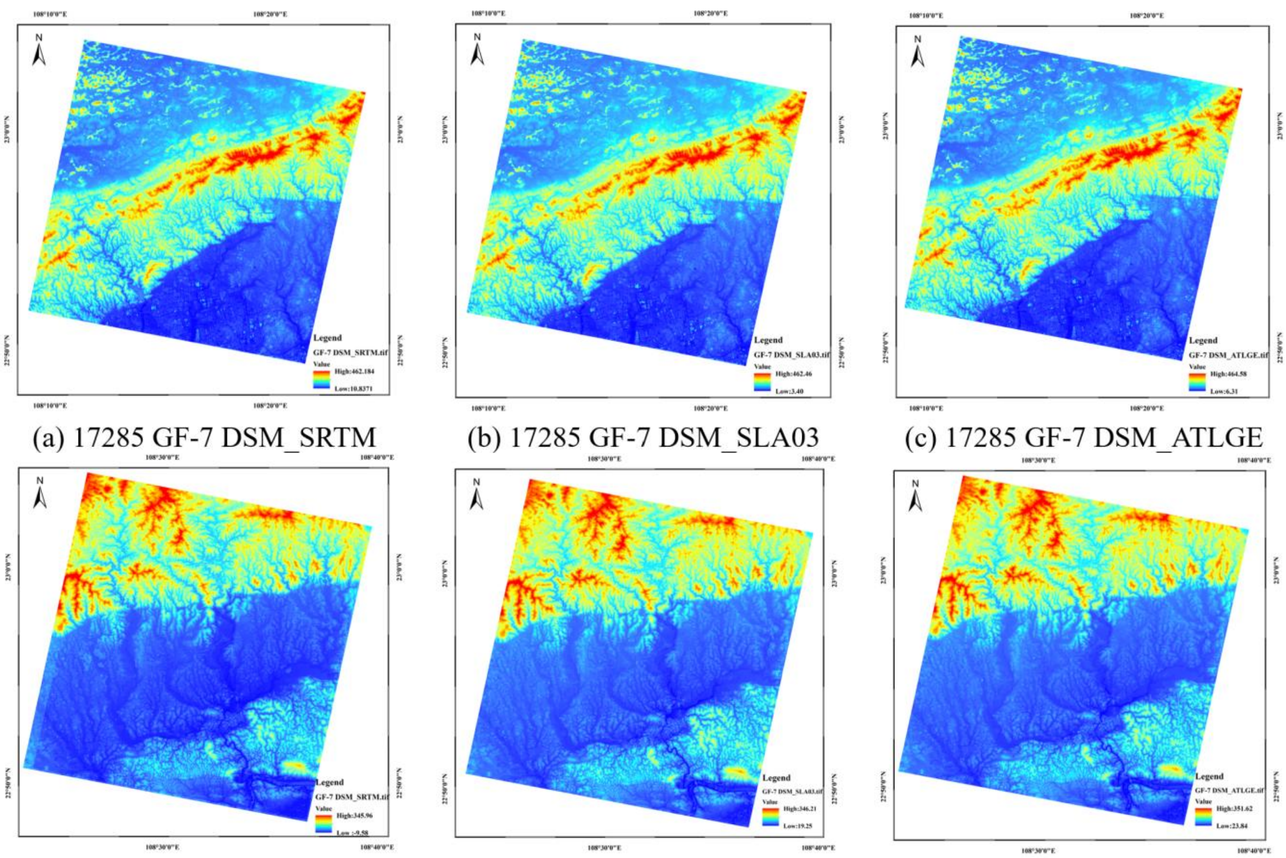

(a) 17285 GF-7 DSM_SRTM (b) 17285 GF-7 DSM_SLA03 (c) 17285 GF-7 DSM_ATLGE

(d) 4606 GF-7 DSM_SRTM (e) 4606 GF-7 DSM_SLA03 (f) 4606 GF-7 DSM_ATLGE

https://doi.org/10.5194/isprs-annals-X-G-2025-981-2025 |

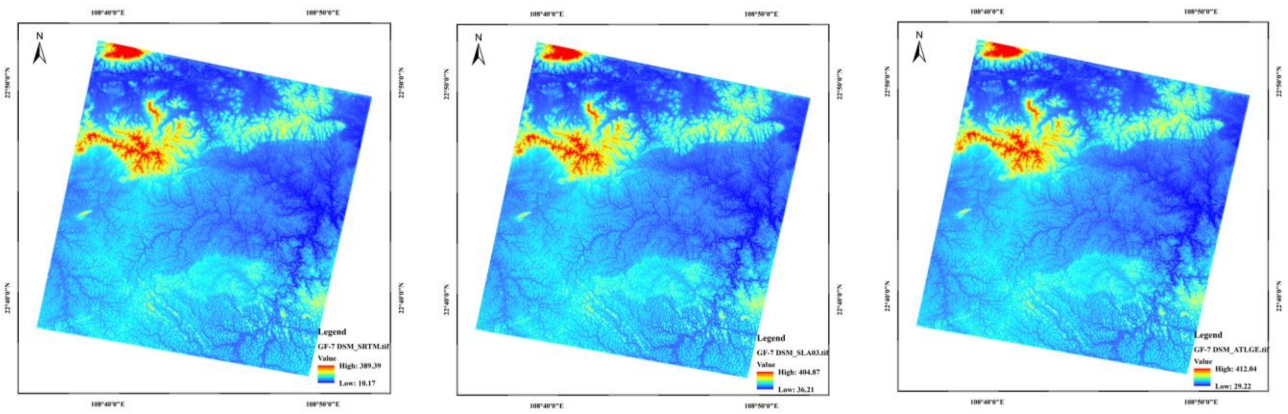

(g) 13644GF-7 DSM_SRTM (h) 13644 GF-7 DSM_SLA03 (i) 13644 GF-7 DSM_ATLGE

Figure 5. DSMs generated under different elevation control conditions of GF-7 stereo images

GF-7 DSM ID	Plot ID	Elevation Difference(m)		
		GF-7 DSM_SRTM	GF-7 DSM_SLA03	GF-7 DSM_ATLGE
17285	ZB087	4.34	2.60	1.57
	ZN004	7.71	3.56	1.73
	ZN005	5.62	2.30	-0.13
	ZN009	5.15	2.10	2.11
	ZN013	6.51	2.94	0.14
	ZN012	12.47	8.35	6.20
	ZN06	4.49	1.81	0.46
	ZN064	6.22	2.15	1.42
	ZN066	6.97	3.90	3.72
	ZN072	7.46	3.75	1.65
	ZN08	4.38	0.90	-0.09
	ZN081	4.40	2.86	2.40
	ZN086	5.45	1.98	1.53
	ZN088	4.38	0.90	-0.09
	ZN090	5.23	1.00	0.10
	ZN091	5.39	3.36	3.24
	ZN093	5.73	1.76	-0.33
	ZN095	7.41	3.60	1.33
	ZN096	4.18	1.28	-0.08
	ZN097	3.70	1.46	0.03
	ZN098	6.06	3.34	2.92
	ZN65	6.39	3.12	2.87
4606	GX023	6.73	3.70	2.57
	GX028	12.93	9.76	3.57
	GX029	11.40	7.48	1.39
	GX031	9.43	6.09	1.75
	GX039	9.85	6.66	1.71
	GX084	11.28	7.46	5.54
	GX085	10.26	7.24	3.09
13644	BLZ14	30.61	11.33	10.67
	WX010	23.12	4.12	2.56
	WX011	24.02	4.60	1.42
	WX012	24.71	5.33	1.81
Bias/m		9.21	4.02	2.08
RMSE/m		11.87	4.78	2.99

Table 1. Elevation accuracy verification results of GF-7 DSM_ATLGE, GF-7 DSM_SRTM, and GF-7 DSM_SLA03

https://doi.org/10.5194/isprs-annals-X-G-2025-981-2025 | © Author(s) 2025. CC BY 4.0 License.

4.3 Abnormal Survey Plots Analysis

From Table 1 and Figure 6, it is evident that the elevation differences between the field-surveyed plots GX084, ZN012, BLZ14 and the corresponding regions in the three DSMs were significantly higher than those in the other plots. These three plots were thus regarded as abnormal plots for elevation accuracy validation. To further explore the reasons, a multi-faceted analysis was conducted, focusing on factors such as feature diversity, elevation differences, slope range, and fractional vegetation cover（FVC）in the abnormal plots.

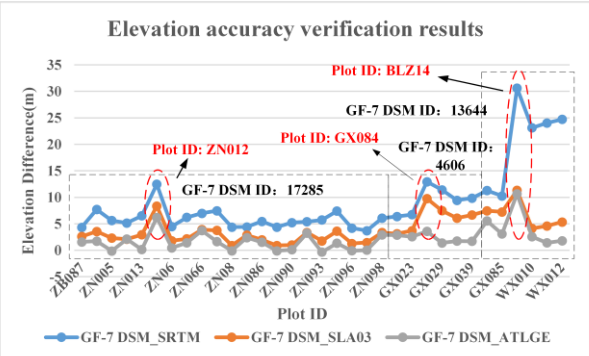

Figure 6. Elevation accuracy verification results of GF-7 DSM_ATLGE, GF-7 DSM_SRTM, and GF-7 DSM_SLA03

(1) During the process of DSMs elevation accuracy verification, this study used the average elevation of the plots as their representative elevation. Similarly, the average elevation within the corresponding DSMs regions was taken as the elevation to be validated. When there are significant variations in elevation and slope within a plot, this averaging method may lead to certain errors. As shown in Figure 7 the internal elevation differences in the three plots exceeded 17 m, with ZN012 exceeding 24.11 m, which is higher than the vast majority of other field-surveyed plots. Additionally, the slope range in all three plots exceeded 78°, with no significant difference from the other plots. Although the slope variation was not particularly abnormal, the large elevation differences might be one of the reasons for the abnormal results in the elevation accuracy validation.

(2) As shown in Figure 8 (a)(b)(c), by referring to GE, the three abnormal plots are all covered by forests, with no significant changes in ground objects within the plots. However, due to the time gap between the DSMs and the field-surveyed plots, plots located in less stable areas may show significant elevation discrepancies compared to the DSMs. For example, plot GX084 is situated near a road, where instability caused by pedestrians or vehicles could result in a large elevation difference between the plot and its corresponding DSMs.

(3) Considering that during push-broom stereo imaging by GF-7, in areas with low FVC, the forward and backward cameras may misinterpret objects beneath the canopy, such as tree trunks, as the canopy top due to the tilt angle of the imaging, leading to an underestimation of elevation of the regions. Therefore, this study calculated the FVC of all plots, with most reaching 100%. However, the FVC for the three abnormal plots was 97.17% (GX084), 98.21% (ZN012), and 93.67% (BLZ14), all below 100% (Figure 7). Therefore, there is a certain probability that the elevation of the objects will be underestimated due to the tilt angle of stereo imaging.
Based on the above reasons, this study suggests that the reason for the abnormality when the three plots are used as reference data is the combined influence of elevation changes, vegetation coverage and geographical location within the plots. This influence may be a common problem in the process of stereo mapping to produce DSM.

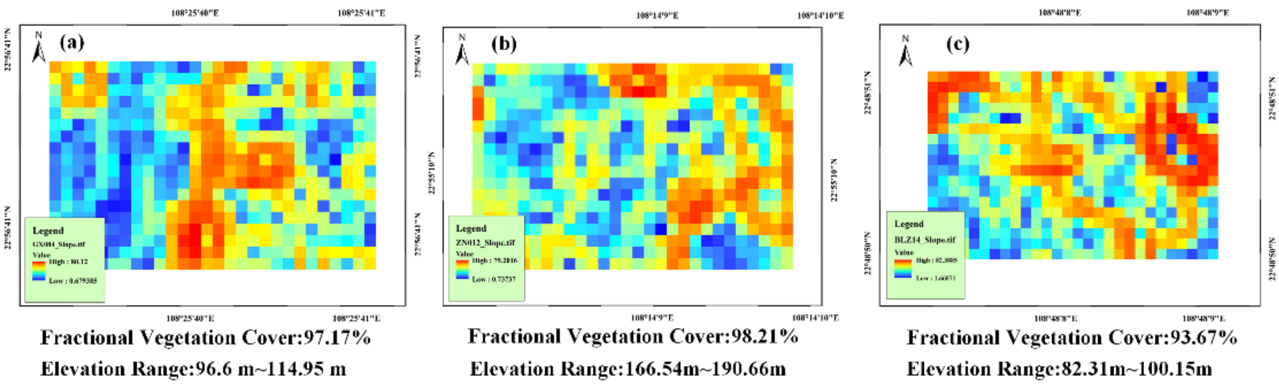

Figure 7. Abnormal plots slope, elevation range and FVC

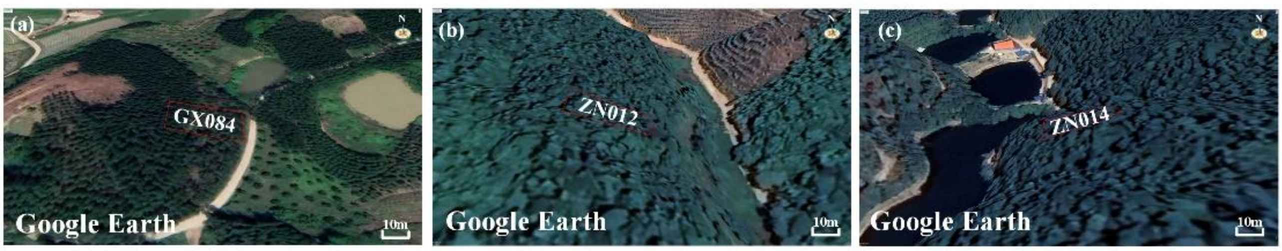

Figure 8. The feature types and geographical location display of abnormal plots

5. Conclusions

Due to the complex terrain and vegetation in forested areas, along with the challenges of obtaining field survey control points, acquiring high-precision DSMs for mountainous forest regions using GF-7 stereo images presents significant difficulties. This study used ATLAS/ICESat-2 as the research object, combined the ground surface detection method based on direction adaptive OPTICS with GE, to finely screen a small number of ATLGE GCPs in forested areas. ATLGE GCPs were used as elevation controls to generate the GF-7 DSM_ATLGE in combination with GF-7 stereo images. To explore the potential of ATLGE GCPs in improving DSM elevation accuracy, SRTM and SLA03 were also introduced as elevation controls, generating GF-7 DSM_SRTM and GF-7 DSM_SLA03 for accuracy comparison. Using 34 field-surveyed plots as reference data, the elevation accuracy of the three DSMs was quantitatively assessed, indirectly evaluating the potential of ATLGE GCPs to enhance DSM accuracy. The results indicated that:

The elevation RMSE of GF-7 DSM_SRTM exceeded 11.87m. After introducing SLA03 laser data, the elevation accuracy of the GF-7 DSM_SLA03 was significantly improved to 4.78m. When ATLGE GCPs were used as elevation control points, the elevation accuracy of the GF-7 DSM_ATLGE was further enhanced to 2.99m, thus improving the usability of GF-7 stereo mapping in forested areas.

Compared to SLA03, a smaller number of ATLGE GCPs can effectively enhance the accuracy of the DSM. Moreover, the higher precision and density of ATLAS offer more options for extracting reliable ATLGE GCPs.
In summary, this study explored the potential of using a limited number of ATLGE GCPs to enhance the accuracy of GF-7 stereo mapping. However, several limitations remain: when the study area is fully covered by continuous, dense forest without any bare land, the ATLGE GCPs extraction method becomes inapplicable. Therefore, obtaining reliable GCPs from ATLAS in areas without bare land will be a key focus for future research.

References

Du, L., Pang, Y., Ni, W., Liang, X., Li, Z., Suarez, J., and Wei, W., 2023. Forest Terrain and Canopy Height Estimation Using Stereo Images and Spaceborne LiDAR Data from GF-7 Satellite. Geo-spatial Information Science. 27(3), 811–821.
Fraser, C., and Hanley, H., 2005. Bias-compensated RPCs for sensor orientation of high-resolution satellite imagery. *Photogrammetric Engineering and Remote Sensing*. 71(8), 909–915.

Grodecki, J., and Dial, G., 2003. Block Adjustment of High-Resolution Satellite Images Described by Rational Polynomials. Photogrammetric Engineering and Remote Sensing. 69, 59-68.
Liu, C., Cui, X., Guo, L., Wu, L., Tang, X., Liu, S., Yuan, D., Wang, X., 2022. Satellite Laser Altimetry Data-Supported High-Accuracy Mapping of GF-7 Stereo Images. *Remote Sensing*. 14, 5868.

Ni, W., Li, Z., Wang, Q., Zhang, Z., Liu, Q., Pang, Y., He, Y., Li, Z., Sun, G., 2024. Forest Height Extraction Using GF-7 Very High-Resolution Stereoscopic Imagery and Google Earth Multi-Temporal Historical Imagery. *Journal of Remote Sensing*. 4:0158.

Xie, J., Yang, X., Xu, C., Lu, Y., Zhang, L., Mo, F., Lv, X., Liu, R., Zeng, J., 2024. Ground and canopy surface detection method based on direction adaptive OPTICS in mountainous forest area. *National Remote Sensing Bulletin*. 1-16.

Zhou, P., Tang, X., Wang, Z., Cao, N., Wang, X., 2018. SRTM-assisted block adjustment for stereo pushbroom imagery. *The Photogrammetric Record*. 33, 49–65.

Zhu, X., Ren, Z., Nie, S., Bao, G., Ha, G., Bai, M., Liang, P., 2023. DEM Generation from GF-7 Satellite Stereo Imagery Assisted by pace-Borne LiDAR and Its Application to Active Tectonics. *Remote Sensing*. 15, 1480.

Zhu, X., Tang, X., Hu, W., Liu, B., Zhang, G., Pan, H., 2024. Accuracy Assessment of GF-7 Geolocation Without GCPs Considering Atmospheric Refraction and Aberration of Light. *IEEE Transactions on Geoscience and Remote Sensing*. 62, 1-15.

https://doi.org/10.5194/isprs-annals-X-G-2025-981-2025